Control of Particle Distribution in Inkjet Printing through an Evaporation-Driven Sol–Gel Transition

Emma L. Talbot,[†] Lisong Yang,[†] Arganthaël Berson,[‡] and Colin D. Bain[*,†]

Department of Chemistry, Durham University, Durham, DH1 3LE, United Kingdom, and School of Engineering and Computing Sciences, Durham University, Durham, DH1 3LE, United Kingdom

E-mail: c.d.bain@durham.ac.uk

Phone: +44 (0)191 3342138. Fax: +44 (0)191 334 2051

Abstract

A ring stain is often an undesirable consequence of a droplet drying. Particles inside evaporating droplets with a pinned contact line are transported towards the periphery by radial flow. In this paper, we demonstrate how suspensions of laponite can be used to control the radial flow inside picolitre droplets and produce uniform deposits. The improvement in homogeneity arises from a sol–gel transition during evaporation. Droplets gel from the contact line inwards, reducing radial motion of particles and thus inhibiting the formation of a ring stain. The internal flows and propagation of the gelling front were followed by high-speed imaging of tracer particles during the evaporation of picolitre droplets of water. In the inkjet nozzle, the laponite network

[*]To whom correspondence should be addressed

[†]Department of Chemistry, Durham University, Durham, DH1 3LE, United Kingdom

[‡]School of Engineering and Computing Sciences, Durham University, Durham, DH1 3LE, United Kingdom

is broken down under high shear. Recovery of the low shear viscosity of laponite suspensions was shown to be fast with respect to the lifetime of the droplet, which was instrumental in controlling the deposit morphology. The radial and vertical particle distributions within dried deposits were measured for water droplets loaded with 1%w and 5%w polystyrene spheres and various concentrations of laponite. Aggregation of the polystyrene spheres was suppressed by addition of colloidal silica. The formulation can be tuned to vary the deposit profile from a ring to a pancake or a dome.

Keywords

coffee ring, droplet deposition, inkjet printing, profile control, laponite additive, sol–gel transition

Introduction

Inkjet printing is a widely used non-contact method for delivering colloidal suspensions onto substrates.[1] A uniform particle distribution in the deposit is usually desired. For example, in graphical printing, a uniform deposit requires the minimum amount of ink for a given colour density. A contact line that is pinned at a constant radius is also desirable to produce a well-defined edge to the deposit: contact lines that retract during drying often lead to irregular deposits and poorly controlled properties. Pinning is common on rough[2,3] or chemically inhomogeneous substrates,[4,5] and for fluids containing high solid loadings.[6–8]

While a uniform particle distribution is the ideal, often a ring stain is the reality.[9–13] For a sessile droplet with a contact angle less than 90°, evaporation is greatest at the contact line. If the contact line is pinned, fluid flows towards the periphery replenishing liquid lost due to evaporation.[14] Particles inside the droplet are transported to the contact line and build up a ring stain (the "coffee ring effect").[9] Particle migration within drying droplets can also produce a non-uniform deposit.[15,16] A non-uniform particle distribution reduces the

quality of graphical printing, since the optical density varies across the deposit. Similarly, printed electronics are limited by variation of the conductivity or porosity across a printed feature.[17–19] Biological assays based on inkjet technology also need a uniform concentration of material across the deposit to be most effective.[20]

A number of methods have been proposed to suppress ring stains. Mechanical methods such as selective laser sintering[21] or multiple passes of the print-head adjust the profile of the end deposit through physical addition or removal of material. Schirmer *et al.* filled in the ring stains using multiple droplets, each forming a smaller concentric ring stain.[22]

Other methods exploit the underlying solvent properties or include additives to alter the flow pattern. Reducing the radial flow, or changing the flow pattern from radial to circulating, inhibits the formation of a ring stain by limiting the supply of colloidal material to the contact line. Radial flow has been reduced or prevented by adjustment of the solvent composition in the ink,[13,23–26] by control of the substrate temperature,[27,28] or by a combination of flow manipulation and contact line de-pinning using electro-wetting.[29–31]

Surface-tension gradients change the internal flows within drying droplets. These "Marangoni effects" produce a recirculating closed cell.[32–34] The cell transports particles away from the contact line and counteracts the build-up of a ring stain. Thermal Marangoni flows may arise on heated/cooled substrates,[27,28] or through evaporative cooling.[32,35] Alternatively, solutal Marangoni flows can occur in solvent mixtures,[15,23,36,37] or in the presence of surfactants.[24,38,39] However, when the droplet becomes thin, the evaporation-driven capillary flow may overcome the Marangoni flow, producing a ring stain.[15]

Increasing the viscosity of the droplet during drying is an appealing way of suppressing the ring stain. However, unless the increase in viscosity overcomes the capillary flow a ring stain will still result. The capillary number, Ca, describes the ratio of viscous effects to surface tension,

$$Ca = \frac{\mu v}{\sigma}, \tag{1}$$

where σ is the surface tension, μ is the viscosity and v is the fluid velocity. The order of

magnitude of the velocity is $R/t_{\rm dry} \backsim 10^{-5}$ m s^{-1}, where R is the droplet radius ($\backsim 10^{-5}$ m in inkjet printing) and $t_{\rm dry}$ is the drying time (a few seconds for water). The capillary number must approach one in order for viscous effects to become significant. If $Ca \geq 1$, then the droplet can deform from a spherical cap. For water, $Ca = \left(10^{-3}\ \text{Pa s} \times 10^{-5}\ \text{m s}^{-1}\right)/10^{-1}$ N m^{-1} $\backsim 10^{-7}$; a 10^7-fold increase in viscosity during drying is required to suppress radial flow. The upper viscosity limit for inkjet printing is of the order 10^1 mPa s at shear rates between 10^4–10^6 s^{-1} (depending on whether drop-on-demand or continuous inkjet systems are used), so even this extreme case requires a million-fold increase in viscosity.

An alternative strategy for suppressing the ring stain is to exploit the elastic (rather than the viscous) properties of complex fluids. In order to overcome the capillary flow and prevent particle motion, the elastic modulus of a viscoelastic fluid must exceed the capillary pressure (estimated by the Laplace pressure). We define a dimensionless number

$$\epsilon = \frac{G' r_{\rm c}}{2\sigma}, \tag{2}$$

as the ratio of the elastic modulus, G', to the Laplace pressure ($P = 2\sigma/r_c$) inside the droplet, where $r_{\rm c}$ is the radius of curvature of the droplet. In order to resist deformation, ϵ must be at least of the order 1. For a water-based droplet with contact angle 20° and radius 80 μm, the height, $h \backsim 14\,\mu$m, and the corresponding radius of curvature, $r_{\rm c}$ is 234 μm ($r_{\rm c}=(R^2+h^2)/2h$ where h is the droplet height). Achieving $\epsilon=1$ for a water droplet ($\sigma=72.5$ mN m^{-1} at 20°C) corresponds to an elastic modulus of $G' \backsim 620$ Pa. Note that the capillary pressure decreases during drying (as the radius of curvature increases) so this is only an initial estimate for G'. A G' value of 620 Pa is more likely to be achievable than a viscosity increase of the order of 10^6. A phase transition is employed to achieve a sufficiently large elastic modulus when printing molten waxes or UV-cured inks.[40]

Alternatively, elasticity can be introduced into a viscous fluid by a "sol–gel" transition. A sol is a stable suspension of colloidal particles in a fluid. A gel is a complex fluid/soft solid

that has elastic properties at rest but flows under shear. In a sol–gel transition, colloidal particles aggregate to form an elastic network that percolates through the fluid. A thermally activated sol–gel transition has previously been used to suppress radial convection. Printing onto a heated substrate (when the fluid gels upon heating[41,42]), or printing heated droplets onto a cool substrate (when the fluid gels upon cooling[43]) have both been demonstrated.

Radial convection is the cause of undesirable ring stains. However, if the particles do not move at all, the final deposit will be thickest at the centre and thinnest at the edge (a dome). This profile results from the initially uniform particle distribution collapsing down as a 2D projection during drying. To produce a uniform particle distribution in the final deposit, a controlled amount of radial motion is required: too much radial flow and a ring stain forms, too little and a dome results. The necessary radial motion must therefore be switched-off after an appropriate time.

We have used dilute suspensions of laponite (a nano-particulate clay) to induce a sol–gel transition during evaporation at a constant temperature. As the laponite suspension becomes more concentrated inside a drying droplet, the elastic modulus of the suspension increases,[44] forming a gel capable of resisting the capillary stresses that otherwise result in particle motion. The elasticity of the gel results from the "house of cards" structure formed by the assembly of the plate-like laponite particles with their negatively charged faces and positively charged edges into a network. Variation in the initial laponite concentration allows us to induce gelling after a controlled amount of evaporation. Thus, the extent of radial motion of the particles can be varied to control the final distribution of the deposit. The network breaks down when a shear force is applied, reducing the viscosity and allowing laponite suspensions that are highly viscous gels at low shear rates to be jetted in an inkjet print-head. The shear-thinning properties of laponite suspensions are also desirable for reducing satellites.[45]

As water evaporates from a droplet, the concentration of solute (e.g. laponite) within the droplet increases, but this increase is not uniform. In the absence of convection, the concentration is highest at the air-water interface, leading to the formation of a skin if

diffusion is too slow to redistribute the solute over the thickness of the droplet. Evaporation is fastest at the contact line where the drop is thinnest.[46] Consequently, the concentration of laponite increases from the apex to the contact line, and so gelation starts at the contact line and propagates inwards.

In this paper, we show that the sol–gel transition in laponite suspensions can be used to suppress radial flow and form a uniform deposit. We compare the behaviour of laponite suspensions with a water-soluble polymer of similar low shear viscosity (hydroxyethylcellulose) and show that laponite is more effective at suppressing ring stains.

Experimental

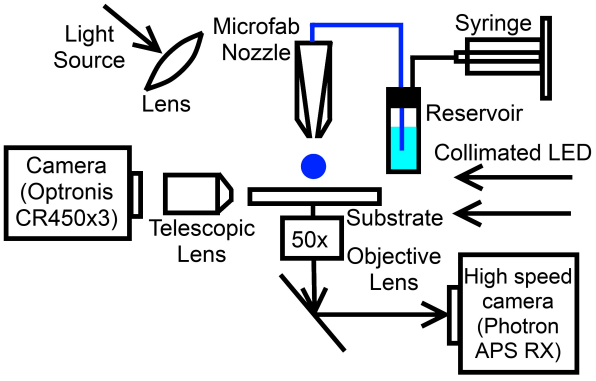

Figure 1. Cartoon of the experimental set-up. The set-up combines an inverted microscope with side-on shadowgraph imaging to view the internal flows and droplet profile simultaneously.

Figure 1 shows the experimental set-up used to image drying picolitre droplets. Views of the side profile of the droplet and internal flows were recorded simultaneously. High-speed shadowgraph imaging was used to capture the side-profiles of the droplets with a mid-speed camera (Optronis CR450x3, frame rate 250 fps, exposure time 2 ms). A cold LED source was used for illumination (455 nm, Beaglehole Instruments) to prevent thermal gradients across the droplet. A custom-written MATLAB routine was used to extract the evaporation rate, diameter, height and contact angle of each droplet.

The internal flows inside drying droplets were recorded on an inverted microscope. Illu-

mination was provided by a cold LED source (530 nm, Thorlabs), focused onto the substrate from above, at an angle (chosen to maximize image contrast). Polystyrene tracer particles were visualized as bright spots (from back-scattered light) on a dark field. Images were acquired using a high-speed camera (Photron APX RS, frame rate 500 fps, exposure time 100 μs, resolution 0.4 μm$\times$0.4 μm) from below, through the substrate. Particle velocities were calculated using particle tracking velocimetry code adapted from routines developed at Georgetown University.[47] The centre of each particle was located and tracked through subsequent frames. Particle velocities were binned radially in increments of $0.1R$ and temporally by $0.1t_{\mathrm{dry}}$, where R is the contact radius of the droplet and t_{dry} is the drying time. The drying time is defined as the time for the droplet volume to reach zero (determined by MATLAB post-processing of the shadowgraph images and confirmed by visual inspection of the inverted microscope images). The contact radius depends on the particle position if the contact area is elliptical: R is the length of the line from the centre of the droplet to the contact line, passing through the location of a given particle. The mean radial velocity (in the x-y plane), $v_{\mathrm{r}}(t)$, was then found for each radial bin. The tangential velocity was negligible unless the contact line de-pinned. Contact radii were found from fitting an ellipse to the particles at the contact line.

Picolitre droplets were ejected from a Microfab (AJ-ABP-01) drop-on-demand device, with an 80-μm orifice, controlled with a Microfab driver unit (Microfab JetDrive III Controller CT-M3-02). The waveform used to eject droplets was adjusted to emit droplets with an impact velocity of $\backsim$ 1 ms^{-1} without satellites. The corresponding approximate shear rate inside the nozzle can be estimated as $u/R \backsim 1$ ms$^{-1}/40\times10^{-6}$ m $\backsim 2.5\times10^{4}$ s^{-1}, where u is the velocity of ejection and R is the radius of the nozzle orifice. Droplets dried at an ambient temperature of 21 °C and a relative humidity of 50%.

Glass cover slips were used for the deposition due to the need for a transparent substrate. The cover slips were used as received, or pre-cleaned with isopropanol to produce a more wetting substrate. Contact angles on glass substrates can vary by $\pm10°$. Dried deposits

were sputter coated with gold (five coats at 1.2 kV, 35 mA for 30 s) before imaging with a scanning electron microscope (SEM, Philips XL30 Environmental SEM). A white light interferometer (Zygo NiewView 5000) provided vertical profiles of the dried deposits. The vertical noise for the interferometer was approximately ± 20 nm. The vertical profiles of the deposits were azimuthally averaged in MATLAB.

To determine the coverage, the images of the deposits were first converted into binary form (using a threshold grey-level just above the background value). The coverage was not sensitive to small variations in the threshold value. The ellipse enclosed by the contact line was sectioned into ten concentric ellipses of equal separation. The fractional area of coverage, ϕ_{n}, where n indicates the ring number (one for the innermost ring), was determined from the number of white pixels within the annulus, divided by the total number of pixels in the annulus. The total area of coverage, ϕ_{t}, is defined by the total number of white pixels divided by the total number of pixels within the ellipse fit to the deposit periphery. The normalised fractional area of coverage within ring n is then $\phi_{\mathrm{n,\,norm}} = \phi_{\mathrm{n}} \,/\, \phi_{\mathrm{t}}$.

Suspensions of laponite RD (Rockwood, 30 nm long disks, 1 nm thick, according to manufacturers specification) in water (MilliQ, 0.25 μm filter) with 0%w, 1%w, 2%w and 3%w laponite content and containing 0.05%w 1-μm sterically stabilised polystyrene spheres (PEGMA-stabilised, zeta-potential -25 to -39 mV for pH 6–9, University of Leeds, UK) were prepared for particle tracking studies. The suspension of polystyrene spheres was made first and the laponite was subsequently added. The laponite powder was fully hydrated and solutions were sonicated for 15 minutes prior to use. No large aggregates were present in the initial formulation. Samples were made fresh on the day of jetting due to the aging properties of laponite suspensions.[48] In order to study deposits from samples with a higher solid content, laponite suspensions were prepared with 1%w and 5%w 200-nm polystyrene spheres. In some formulations, colloidal silica (LUDOX AS-40, Sigma Aldrich, particle diameter $\backsim$ 20 nm, zeta potential $\backsim -75$ mV at pH 7) was included in the laponite suspensions at concentrations up to 1%w as an anti-aggregation agent due to the large-scale aggregates formed in deposits

from laponite suspensions with polystyrene spheres. The colloidal silica was purchased as a stable suspension and was added to the suspension of polystyrene spheres before the laponite powder. The polymer hydroxyethylcellulose (HEC, MW 250 $\mathrm{kg\,mol^{-1}}$, Sigma Aldrich) was tested as a 1%w solution, as this concentration exhibits a similar low shear viscosity to a 2%w laponite solution. Surface tension measurements were collected for each component using a pendant drop tensiometer (First Ten Angstroms, FTA200). Note that problems with clogging did not occur for the suspensions reported in this paper.

Rheological data were collected at 293 K using an AR 2000 Rheometer (TA Instruments) with a cone (2° angle) and plate geometry for laponite suspensions and HEC solutions in water, without the inclusion of polystyrene spheres. The steady-state viscosity of each fluid was recorded over shear rates from 0.1–1500 $\mathrm{s^{-1}}$, where the upper limit was set by the rheometer. The reported steady-state viscosities are an average of three consecutive readings within 2% of each other, and a maximum measurement time of 5 min per reading. Recovery times were investigated by applying a stepped shear rate with fast sampling. The shear rate was held at 0.1 $\mathrm{s^{-1}}$ for 10 minutes, then 1000 $\mathrm{s^{-1}}$ for 4 minutes, before returning to the low shear value (0.1 $\mathrm{s^{-1}}$). The yield stress of each laponite suspension was found using oscillatory measurements with small deformations, performed by running a strain sweep (for strain values between the rheometer's lower limit of 2.88×10^{-3} and 0.35) at a frequency of 1 Hz. The yield stress was estimated from the product of the critical strain and the elastic modulus in the linear elastic region. The critical strain was defined as the strain at which a straight-line fit to the linear elastic region and non-linear viscoelastic region intersected.

Results and discussion

Shear rheology of formulations

Figures 2 and 3 present the steady-state shear viscosity of laponite suspensions and hydroxyethylcellulose (HEC) solutions over a range of shear rates. The laponite suspensions were

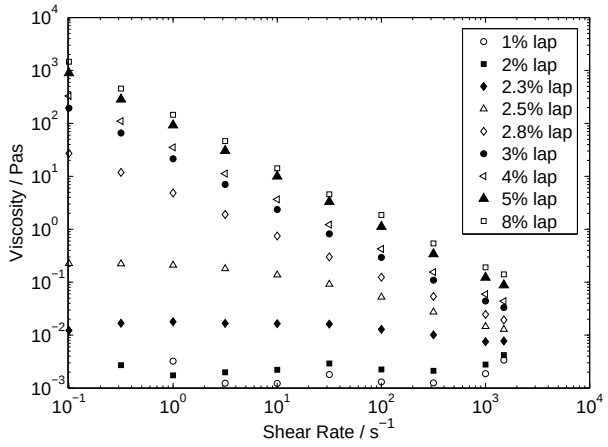

Figure 2. Steady-state shear viscosity of laponite suspensions in water as a function of shear rate.

shear-thinning when the laponite concentration exceeded about 2.5%w. Above 3%w laponite, there was no Newtonian plateau, indicating yield-stress behaviour. The HEC solutions were weakly shear-thinning for HEC concentrations of 3%w and above. Inkjet printed droplets experience high shear rates inside the nozzle (10^4–10^6 s^{-1} in commercial print-heads),[1] and low shear rates (10^0–10^1 s^{-1}) on the substrate. It is therefore necessary to determine if the laponite network can recover during the lifetime of the droplet.

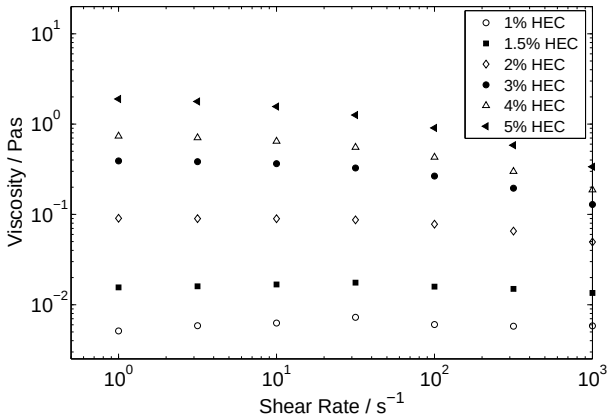

Figure 3. Steady-state shear viscosity of aqueous HEC solutions as a function of shear rate.

Figure 4 shows the recovery of the shear viscosity of laponite suspensions following a period of high shear rate. Although the applied shear was an order of magnitude lower than in an inkjet print-head, the network was fully broken down, and so the recovery time

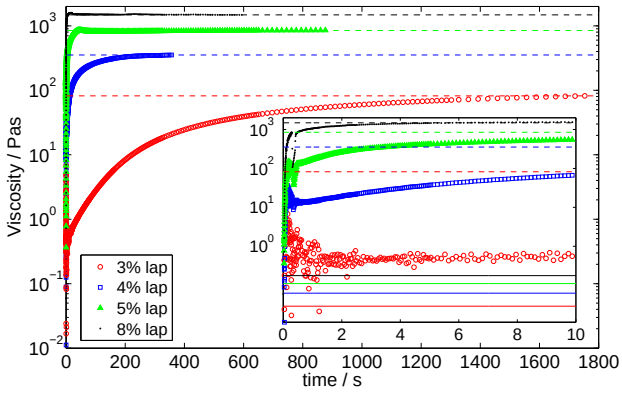

Figure 4. Recovery of the shear viscosity for laponite suspensions over a range of laponite concentrations, following a period of high shear. The inset shows the recovery of the shear viscosity over the first ten seconds, encompassing the typical drying time of inkjet droplets ($\backsim$ 5 s). Dashed horizontal lines indicate the viscosity after full recovery. Solid horizontal lines indicate the viscosity immediately following the switch from high shear rate to low shear rate.

should be the same as if a shear rate of $10^4\,\mathrm{s}^{-1}$ was applied. For laponite concentrations $\gtrsim 3\%$w, the viscosity increased monotonically until the steady-state low-shear viscosity was attained. The recovery of the viscosity was faster for suspensions containing more laponite. For suspensions containing $\leq 5\%$w laponite, the network did not fully recover within the lifetime of a droplet (typically $\backsim$ 5 s). However, there was a significant viscosity increase (of order 10^2) for the 5%w laponite suspension over this time period. Once the laponite concentration reaches 8%w, the suspension fully recovers within seconds (an increase by three orders of magnitude in 5 s, see Fig. 4). During the droplet lifetime, the increase in laponite concentration due to evaporation will therefore facilitate total recovery of the suspension network and the associated elastic properties. While the recovery of the elasticity cannot be directly measured, recovery of the shear viscosity represents the recovery of the networked structure. If the network recovers, we can infer that the elasticity recovers.

Inverted bottle experiments (Fig. 5) show a sol–gel transition between 2.8–3%w laponite. Shear rate versus shear stress curves confirming the concentration range of the sol–gel transition are given in the Supplementary Information (Fig. S1). At 3%w laponite, the suspension had a finite yield stress (see Table 1), and was a shear-thinning gel. The sol-gel transition

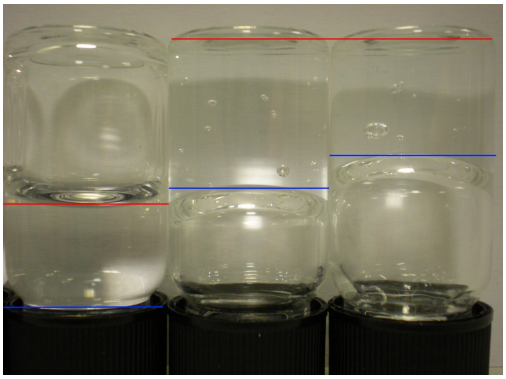

Figure 5. Inverted bottles indicating which laponite concentrations in water are sols and which are gels after leaving overnight. From left to right the laponite concentrations are 2.8%w, 3%w and 4%w. The 2.8%w laponite suspension is a viscous sol. The 3%w and 4%w laponite suspensions are gels trapping bubbles. The blue horizontal lines indicate the lowest lying part of the sample in the vial and the red lines the highest part.

Table 1. Yield stresses determined by oscillatory measurements for laponite suspensions in water at various laponite concentrations.

Laponite concentration / %w	Yield stress / Pa
2.8	0.3
3.0	5
4.0	45
5.0	107
8.0	149

gave rise to a sharp increase in the low-shear viscosity (Fig. 2) and yield stress of the suspension. Note that the addition of 1%w or 5%w 200 nm polystyrene spheres gave a sol–gel transition between 2.5%w laponite (viscous sol) and 3%w laponite (gel) after the same time period (overnight). The sol–gel transition remained between 2.8–3%w laponite on the addition of 1%w colloidal silica.

For our droplets, (typical contact angle $\backsim 20°$, contact radius $\backsim 80\mu$m), the initial capillary pressure is $p_{Ca} \backsim 2\sigma \ / \ r_c \backsim 620$ Pa, where σ is the surface tension of the fluid and r_c is the radius of curvature of the droplet. The gradient in capillary pressure that must be overcome to prevent particle motion is lower than this value. A yield stress of $\backsim 10^2$ Pa is therefore required to overcome capillary flow via network elasticity (giving $\epsilon = 1$ in equation 2). Table 1 indicates that yield stresses of this magnitude occur for laponite concentrations of $\geq$5%w. In comparison, a viscosity increase of a million-fold required to overcome capillary flow could

not be achieved without significant solvent evaporation and so would not be achievable early enough in the drying time to prevent a ring stain. Hence, recovery of the elasticity is the important factor. We can infer from the recovery of the shear viscosity that an 8%w laponite suspension can fully recover the networked structure and therefore the elasticity within the lifetime of the droplet.

A comparison with HEC was performed to further confirm the recovery of the laponite suspensions during drying. For HEC, the change in viscosity from high shear to low shear was less than an order of magnitude for any given concentration of the studied solutions. At low shear rates, the viscosity of HEC solutions increased by three orders of magnitude between 1%w and 5%w. At high shear rates the corresponding viscosity increase was smaller ($\backsim 10^2$) and comparable to the increase in high-shear viscosity in laponite suspensions over the same concentration range. Thus, if the laponite network does not recover on the timescale of droplet drying, HEC and laponite may be expected to show similar drying behaviour.

If the increase in laponite concentration during the drying lifetime is sufficient for full network recovery, the suspension will show a large viscosity increase and sol–gel transition. Once the solution becomes a gel, particle motion will be prevented, and the deposits will differ greatly from those containing HEC.

Table 2. Critical strains determined by oscillatory measurements for laponite/silica suspensions in water at various laponite to silica ratios. Note that yield stresses for suspensions without colloidal silica differ from those in table 1 due to different aging times.

Laponite concentration / %w	Colloidal silica concentration / %w	Ratio laponite : silica	Critical strain / %	Yield stress / Pa
3.0	0.0	1:0	4.1	1.7
3.0	1.5	1:0.5	2.9	4.0
3.0	3.0	1:1	2.6	5.1
5.0	0.0	1:0	4.7	60
5.0	2.5	1:0.5	4.4	72
5.0	5.0	1:1	3.7	90

Laponite was observed to cause aggregation of polystyrene latex particles. Colloidal

silica was added to laponite suspensions to inhibit aggregation, but silica also affected the critical strain (table 2). Increasing the ratio of silica to laponite decreased the critical strain, indicating a reduction in the ability of the network to maintain connectivity. The yield stress and speed of the recovery of the network both increased (for a fixed laponite concentration) as the total solid concentration increased (see Supplementary Information Fig. S10).

Table 3. Surface tension values, σ, for each component in water at 20°C.

Component	Water	1%w laponite	2%w laponite	1%w colloidal silica	1%w HEC
σ / $\mathrm{mNm^{-1}}$	72.5	70.4	69.9	70.4	65.4

The surface tension of the laponite or silica suspensions did not differ significantly from that of water (table 3). HEC had the largest influence, lowering the surface tension to $65.4\,\mathrm{mNm^{-1}}$. The small differences in surface tension let us conclude that the influence of laponite and silica on the capillary pressure (and on the elastic modulus required to prevent particle motion) is small.

Evaporation and gellation of printed droplets

Particle tracks (in blue) are shown in Figure 6 for an evaporating droplet of pure water, a 1%w polymer solution and two concentrations of laponite suspensions (2%w and 3%w) printed onto glass cover slips. The initial contact line is indicated by a solid black circle. For pure water (Fig. 6a), the tracks are purely radial until the contact line de-pins near the end of the drying time (indicated by the stationary particles in green at the right-hand side of the droplet in Fig. 6a(iii)). Figure 7a shows the mean radial velocity of the particles as a function of radial distance from the centre of the droplet for various time periods from the end of spreading until the contact line de-pinned (data after contact line de-pinning is shown in the Supplementary Information). The mean radial velocity of the particles increased throughout drying and with increasing distance from the centre of the droplet (apart from the rim).

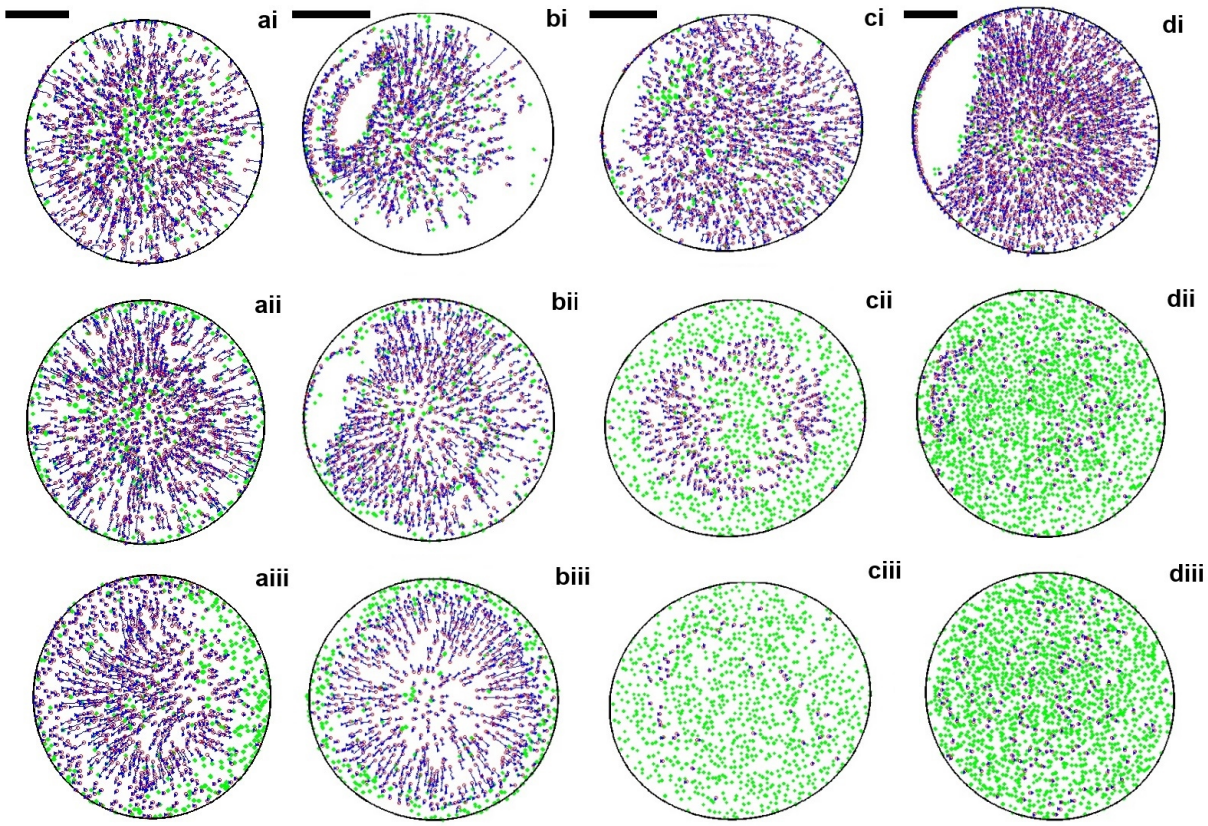

Figure 6. Particle tracks for droplets containing 0.05%w 1-μm polystyrene spheres and a) pure water ($t_{\mathrm{dry}} = 5.03$ s), b) 1%w HEC ($t_{\mathrm{dry}} = 5.02$ s), c) 2%w laponite ($t_{\mathrm{dry}} = 6.32$ s) and d) 3%w laponite ($t_{\mathrm{dry}} = 8.65$ s). The particle tracks are shown for i) 0.0–0.1 t_{dry}, ii) 0.4–0.5 t_{dry} and iii) 0.7–0.8 t_{dry}. Stationary particles (with movement less than two pixels in the time interval) are indicated in green. Moving particles are indicated in blue with a red circle at the start of the track and a blue triangle at the end of the track. The black line indicates the initial contact line. Refraction of light through the droplet prevents dark field imaging in some areas of some images, where no particles are shown. The glass slides were used as-received. The tracks are examples from single representative droplets. Scale bars are 50 μm. Example videos for a drying 2%w laponite suspension and a water droplet are given in the Supplementary Information.

The 1%w HEC droplet (Fig. 6b) exhibited similar flows to the water droplet, with radial flow even at $0.8t_{\mathrm{dry}}$, by which point the mean HEC concentration had reached 5%w and the low shear viscosity had increased by more than two orders of magnitude. The HEC concentration was highest near the contact line leading to a small rim of stationary particles in the final stages of drying (green particles in Fig. 6b(iii)). Figure 7b shows that the velocity profiles for 1%w HEC evolved similarly to pure water, with an increase in the mean radial velocity during drying. However, there was an initial decrease in the velocity at early times,

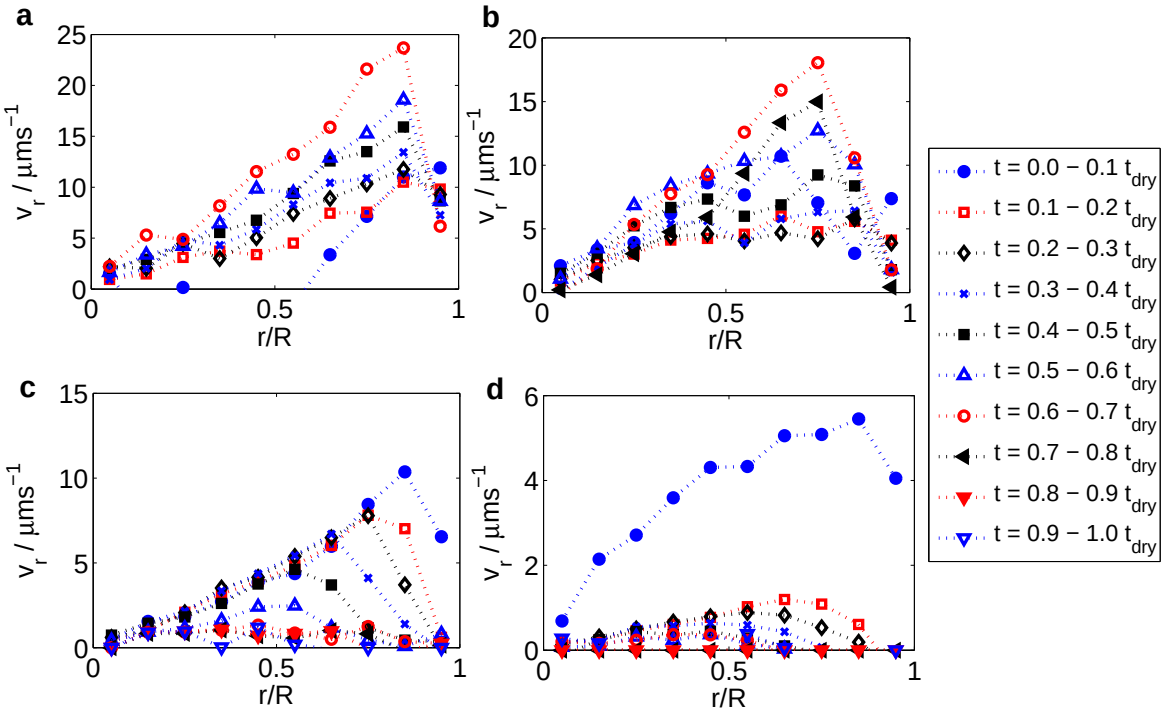

Figure 7. Mean radial velocities, v_r, over the normalised droplet radius are shown for incremented temporal bins for a droplet of a) pure water, b) 1%w HEC, c) 2%w laponite suspension and d) 3%w laponite suspension. Data points are plotted at the mid-point of each spatial bin. For clarity, data are shown for a single representative droplet up until the time that the contact line de-pins (complete data are in the Supplementary Information, see Fig. S2 and Fig. S3).

potentially due to the small amount of motion in the contact line during the first time bin.

The behaviour of particles within a droplet containing laponite was very different. A droplet of 2%w laponite (Fig. 6c) initially showed radial flow throughout the droplet, before a gelling front propagated from the contact line towards the droplet centre. Particles in the gel ceased to move (green particles in Fig. 6c(ii)), while particles in the sol continued to flow radially outwards. During drying, the mean radial velocity of particles within the droplet of 2%w laponite suspension decreased as the gelling front propagated inwards, reducing velocities near the contact line at early times and closer to the centre at later times (Fig. 7c). Additional side images indicating the inward progression of the gelled "disk" and leaving the central sol "cap" can be found in the Supplementary Information (Fig. S7). The deviation of the droplet profile from a spherical cap confirms that the laponite particle network recovers

quickly enough for the sol to gel within the drying time of the droplet ($t_{\mathrm{dry}} \backsim 5$ s). We note that the radial motion within the sol led to a final distribution of tracer particles (Fig. 6c(iii)) that was highly uniform. Particle distributions in dried deposits are discussed in more detail in the following section.

The final set of particle tracks, shown in Figure 6d, are for a 3%w laponite suspension, which forms a shear-thinning gel. Immediately after impact and spreading there was radial flow (Fig. 6d(i)), but gelation rapidly spread throughout the entire droplet and halted particle motion (Fig. 6d). The initial particle motion occurs because there is a finite recovery period after shearing of the gel in the nozzle before the laponite network reforms. We can estimate the recovery time of the gel network to be within 440 ms ($0.1t_{\mathrm{dry}}$) from the time between droplet impact and gelation of the droplet. Figure 7d shows the radial velocity profiles for the 3%w laponite formulation, confirming the formation of a gel within $0.1t_{\mathrm{dry}}$.

For droplets without laponite, the velocity of particles increased during drying and towards the contact line. For droplets containing laponite, the velocity of particles decreased throughout drying, as particles slowed down in the gel. Plots of how the maximum velocity varies radially and temporally are given in the Supplementary Information (Fig. S8 and Fig. S9).

The droplets in Figure 6 were printed onto a cover slip as received from the supplier. These cover slips have varying levels of chemical contamination that increases contact angle hysteresis, leading to pinning of the contact line. If the substrates are cleaned with isopropanol before use, pure water droplets quickly de-pin (Fig. 8a). The receding contact line drags particles inward leaving an irregular and unpredictable deposit shape. The gelled rim of the laponite droplet pins the contact line throughout drying (Fig. 8b) resulting in a circular edge to the deposit with a radius defined by the initial spreading of the droplet on the substrate. As with the droplets printed on as-received glass, the width of the gelled ring grew as evaporation progressed with the freely flowing suspension restricted to a region of

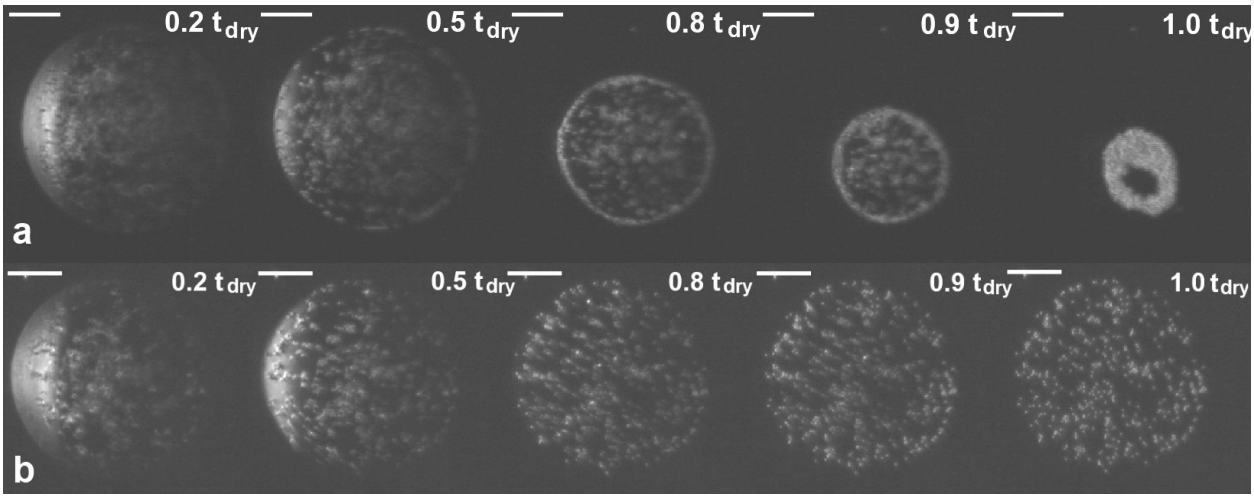

Figure 8. Inverted microscope images for a) a droplet containing 0%w laponite, with 0.05%w 1-μm polystyrene spheres on a glass substrate pre-cleaned with isopropanol, and b) 2%w laponite. For a) the droplet de-pins during drying, but for b) the droplet stays pinned throughout drying. The scale bars are 50 μm.

decreasing radius around the centre of the droplet.

In this section, we have established that laponite controls the amount of radial flow in evaporating droplets. It is the radial flow that is responsible for forming ring stain deposits in drying droplets. However, in order to form a uniform deposit rather than a dome, some radial motion is necessary. The combination of the concentration of the laponite during drying and a fast recovery time of the networked structure is essential to control the extent of radial flow. In the following section, we examine dried deposits to determine if, by using laponite to reduce the radial flow, we can control the particle distribution and eliminate ring stains.

Distribution of tracers in dry deposit

Figure 9 shows scanning electron micrographs of the dried deposits from various formulations containing 0.05%w of 1-μm tracer polystyrene spheres. From these micrographs, we calculated the fraction of the substrate covered by polystyrene spheres as a function of the radial distance from the centre of the deposit. Figure 10 plots these distributions, normalised to the average density. The laponite suspensions provided a more uniform distribution of

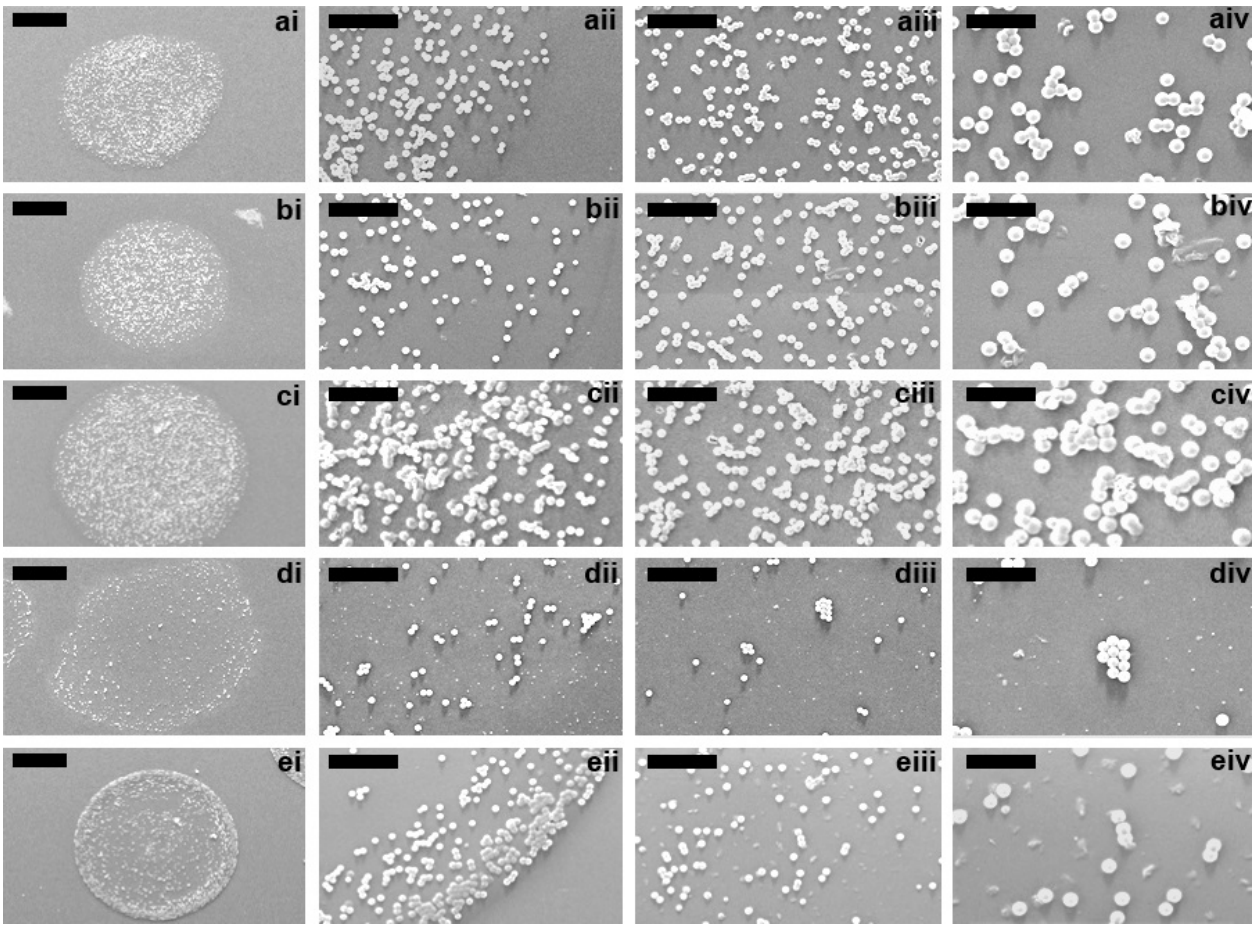

Figure 9. SEM images of deposits containing 0.05%w 1-μm polystyrene spheres: a) 1%w laponite, b) 2%w laponite and c) 3%w laponite, d) pure water, and e) 1%w HEC. Images show i) the whole droplet at 400× zoom (scale bar 50 μm), ii) a 2500× zoom to the contact line (scale bar 10 μm), iii) a 2500× zoom to the interior (scale bar 10 μm), iv) a 5000× magnification of the interior (scale bar 5 μm). Glass substrates were used as-received.

tracer particles than either water or 1%w HEC, both of which show an increase in the particle density towards the edge of the deposit (a ring stain). The 1%w HEC solution also shows a build up of particles at the centre of the deposit. In laponite suspensions containing only a trace amount of solids, the laponite concentration made little difference to the area covered by the deposit. The 1%w, 2%w, and 3%w laponite suspensions produced a uniform density of particles across most of the deposit, except near the contact line where the particle density decreased. (Fig. 9a–c).

Close inspection of the high resolution images (Fig. 9, column iv) show that the diameter of the polystyrene spheres deposited from 3%w laponite appears to be nearly double that in

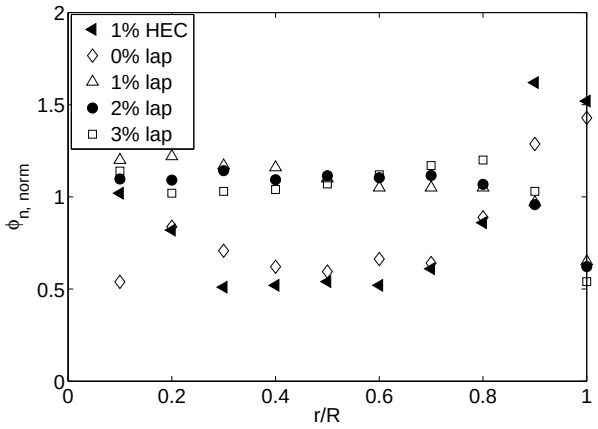

Figure 10. The radial distribution of the deposit consisting of 1-μm polystyrene spheres at 0.05%w solids content. The normalised fractional area of coverage, $\phi_{\mathrm{n,\,norm}}$, is plotted at the outer radial position, r, for each ring i.e. at 0.1 for ring n=1, encompassing r/R = 0–0.1 (where R is the deposit radius). Values are the average of at least twenty deposits.

the pure water. The explanation is that during drying the nanoparticles of laponite coat the polystyrene sphere. The change in size of the spheres is less evident for the lower laponite concentrations, but the outlines of the spheres are less sharp than for the water droplet (Fig. 9d) and the spheres blend into each other where they are in contact, owing to the laponite coating between the spheres. The HEC deposit shows a polymer coating on the spheres near to the contact line where the HEC ring stain forms (Fig. 9(eii)).

Deposits with a high solid content

In the previous section we demonstrated that control of radial flow in laponite suspensions can lead to a uniform coverage of tracers particles in a dried deposit. We now investigate whether the same uniformity can be achieved in formulations with a higher fraction of suspended solids, for which we chose 200-nm polystyrene spheres at concentrations of 1%w and 5%w.

Figure 11 shows SEM micrographs of droplet deposits containing 1%w 200-nm polystyrene spheres. The droplet of water de-pinned during drying and produced a highly non-uniform distribution with a holey structure consisting of patches of covered and bare substrate (Fig.

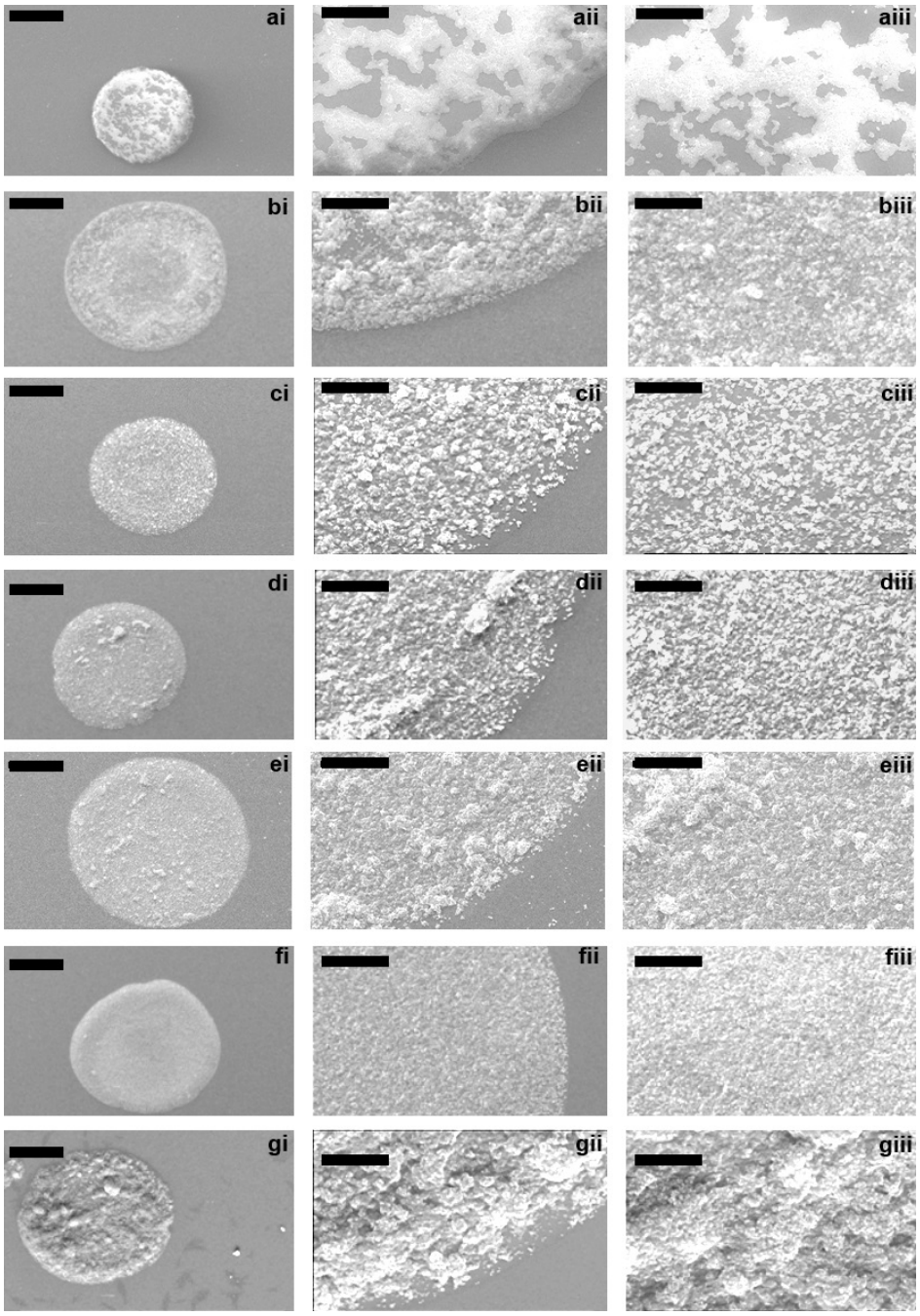

Figure 11. SEM images of deposits containing 1%w 200-nm polystyrene spheres: a) pure water, b) 1%w HEC, c) 2.8%w laponite, d) 2.5%w laponite, e) 2.0%w laponite, f) 2%w laponite with 1%w colloidal silica, and g) 3%w laponite with 1%w colloidal silica. Segments show i) the whole droplet (400× magnification, scale bar 50 μm), ii) a zoom to the contact line (2500× magnification, scale bar 10 μm) and iii) a zoom to the interior (2500× magnification, scale bar 10 μm). Substrates were as-received glass.

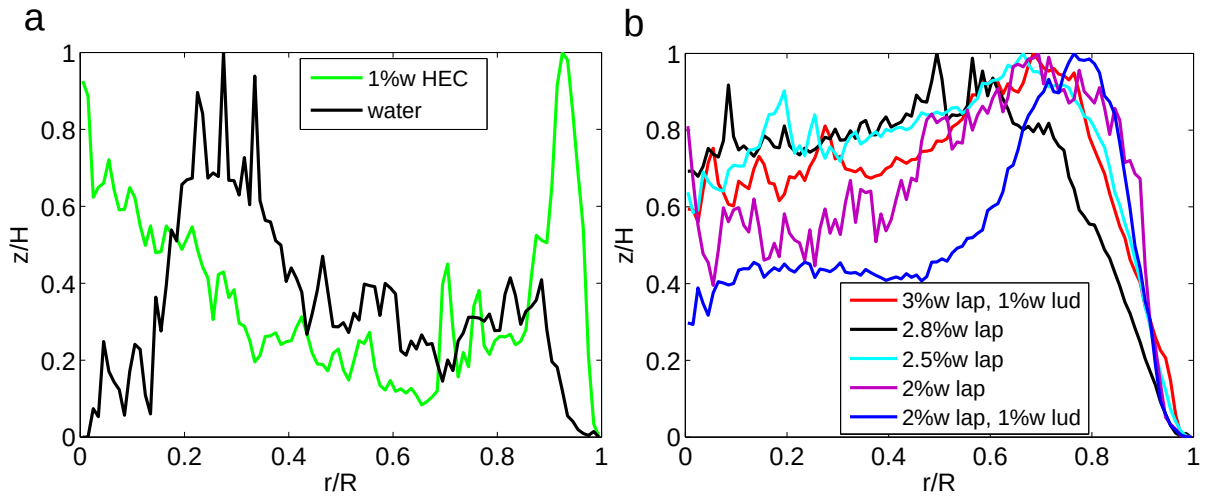

Figure 12. Azimuthally averaged height profiles taken on a white light interferometer, for deposits of a) water droplets containing 1%w 200-nm polystyrene spheres with and without HEC, and b) various concentrations of laponite and colloidal silica. The deposit height, z, at a radius, r, from the deposit centre is normalised by the maximum height of the deposit, H. R is the deposit radius.

11a). The interferometric profile (Fig. 12a) confirmed the non-uniform thickness. As expected, due to the de-pinning, there was no significant ring structure at the contact line. For a droplet containing 1%w HEC, the deposit had a thin ring at the edge and a non-uniform radial profile (Fig 11b). Interferometry revealed that the deposit had a raised central region as well as a ring at the contact line (Fig. 12a). Droplets containing laponite (Fig 11c–e) produced more uniform radial particle distributions with fewer patches. The interferometry profiles show that laponite concentrations of 2.8%w and 2.5%w formed fairly flat deposits (Fig. 12b) while the 2%w suspension had a dip at the centre, indicating that gelation took place too late in the drying process to suppress ring formation completely.

While laponite generated spatially more uniform deposits, it had the negative effect of promoting aggregation of the PS colloids during the drying process as shown by the many large aggregates in Fig 11c–e. A possible explanation is that the laponite plates with positively charged edges can bridge between negatively charged PS spheres. These large aggregates give rise to an undesirable rough texture in the deposits. In order to

suppress aggregation of the PS spheres induced by the laponite, we added 1%w colloidal silica to the 2%w laponite solution. The silica reduced the number of large aggregates and produced a much smoother surface texture (compare Fig. 11e and Fig. 11f). The suspensions containing colloidal silica were less effective at suppressing the ring stain. It is possible that the lower critical strain in suspensions containing silica (table 2) reduces the ability of loose aggregates to remain connected under the gentle shear within the drying droplet. Without connectivity throughout the suspension, the elasticity cannot recover. Consequently, particles move outwards with the radial flow and build-up a ring, similar to pinned droplets without laponite (Fig. 12b). To increase the critical strain, we increased the laponite concentration to 3%w at fixed silica concentration and obtained a fairly uniform pancake deposit (Fig. 12b). However, aggregates formed once again (Fig. 11g) indicating a trade-off between ring-suppression and aggregate-formation dependent on the laponite to silica ratio, which would have to be optimised in an ink formulation.

SEM micrographs of dry deposits formed from suspensions of 5%w PS spheres are shown in Figure 13, with the azimuthally averaged height profiles shown in Figure 14. For both pure water and 1%w HEC, the footprint of the drop was completely covered by polystyrene spheres, but there was a pronounced ring stain (Fig. 13a–b). On addition of 2%w or 1%w laponite, the deposit had a domed morphology with large aggregates (Fig. 13c) or cracking near the periphery (Fig. 13d). The sol–gel transition occurred too quickly to allow sufficient radial motion of the polystyrene particles. The vertical profile of the deposit was then thicker where the droplet was highest. The presence of a high concentration of PS nanospheres appears to reduce the amount of laponite needed to form a gel. Reducing the laponite concentration to 0.8%w delayed gelation and yielded a fairly flat pancake. However, the presence of large aggregates resulted in uneven deposition and a rough surface texture (Fig. 13e). Further addition of 1%w of colloidal silica reduced the peripheral cracking in the 1%w laponite droplet (Fig. 13g) and the number of aggregates in the 0.8%w laponite deposit (Fig. 13h), though aggregates still remained in the 2%w laponite droplet (Fig. 13f).

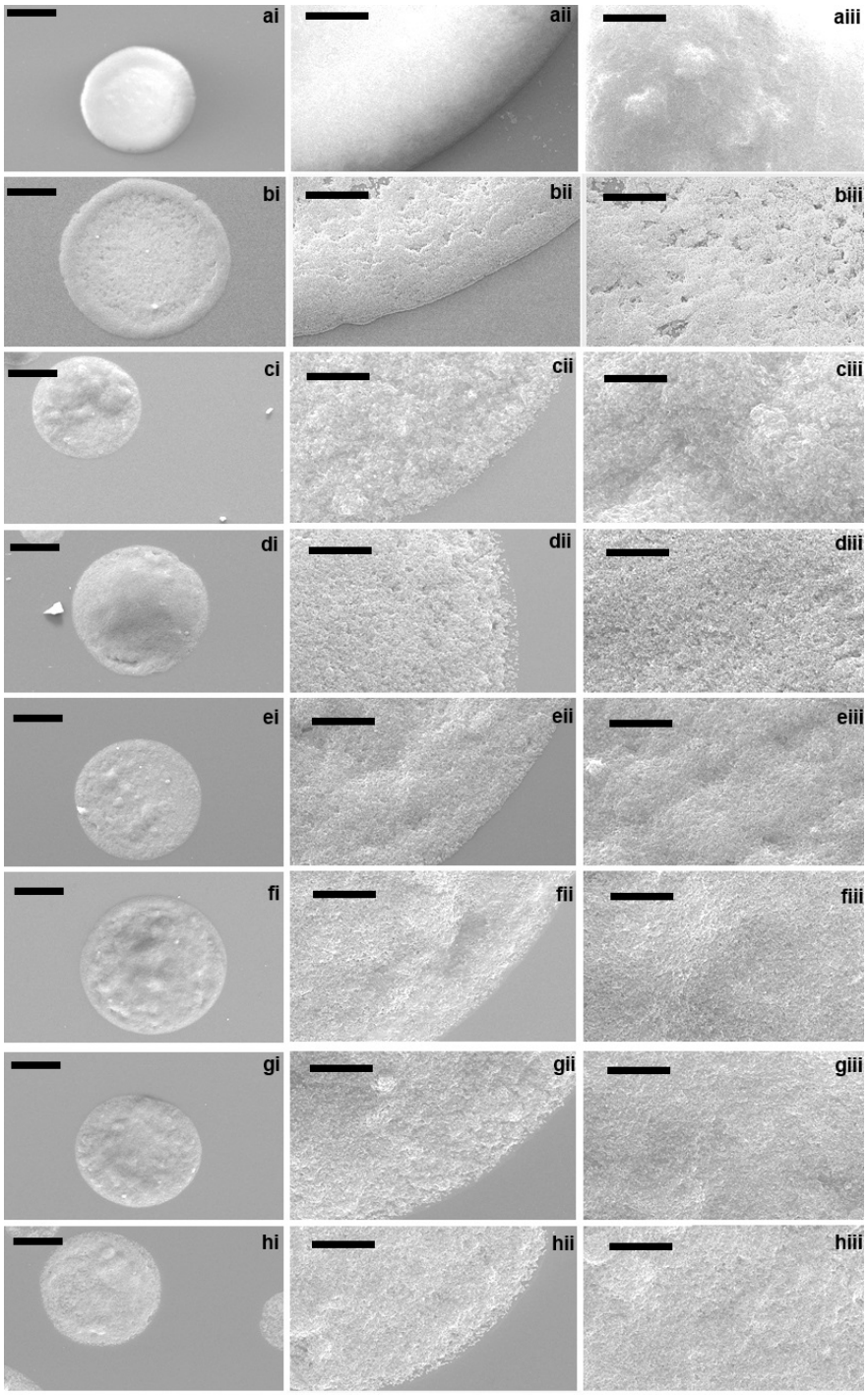

Figure 13. SEM images of deposits containing 5%w 200-nm polystyrene spheres. a) pure water, b) 1%w HEC, c) 2%w laponite, d) 1%w laponite, e) 0.8%w laponite, f) 2%w laponite and 1%w colloidal silica, g) 1%w laponite and 1%w colloidal silica, and h) 0.8%w laponite and 1%w colloidal silica. Segments show i) the whole droplet (400× magnification, scale bar 50 μm), ii) a zoom to the contact line (2500× magnification, scale bar 10 μm) and iii) a zoom to the interior (2500× magnification, scale bar 10 μm). Substrates were as-received glass.

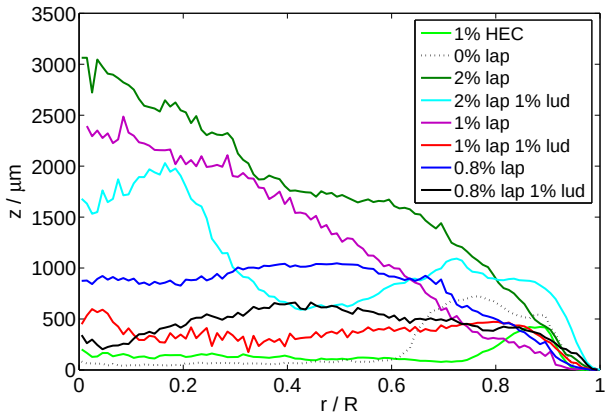

Figure 14. Azimuthally averaged height profiles taken on a white light interferometer, for deposits of water droplets containing 5%w 200-nm polystyrene spheres and either HEC or various concentrations of laponite and colloidal silica. The deposit height, z, at a radius, r, from the deposit centre shown, where the radius is normalised by the maximum radius of the deposit, R.

The networking properties of the laponite/colloidal silica mixtures will depend on the ratio of laponite to colloidal silica and the gelation point also depends on the total solid volume fraction (including the polystyrene spheres). We have not attempted to optimise this formulation, but the flatness and uniformity of the profile formed from the 1%w laponite droplet containing 1%w colloidal silica is already very encouraging.

Conclusions

Formulation of colloidal suspensions for inkjet printing is a complex problem that involves balancing the competing requirements of the fluid. The formulation must be stable during storage, jettable from an inkjet printhead, and it must dry on the substrate to give the desired morphology of the deposit. This paper has focused on the last of these problems, and specifically on counteracting the "ring stains" that arise from convective flow towards a pinned contact line. The capillary numbers in inkjet printed droplets are exceedingly low ($\backsim 10^{-6}$), and an increase in viscosity alone during drying was inadequate to prevent the formation of a ring stain.

Fluids that undergo a sol−gel transition as the concentration of the structuring agent

increases generate elasticity in the fluid. If the yield stress of the fluid exceeds the capillary pressure, then the convective flow to the contact line (which generates the ring stain) may be stemmed. We have shown that an evaporation-driven sol−gel transition in laponite suspensions can be used to control the morphology of a deposit for a model colloidal suspension (comprising sterically stabilised latex spheres). The enhanced evaporation rate near the contact line causes the droplet to gel first at its rim, with the gelled region progressing inwards to the centre of the droplet. By controlling the laponite concentration, and hence the timing of the gelling, we can dictate the amount of radial flow required to generate a uniform deposit: too little radial flow and a domed structure forms, too much and a ring stain is produced.

The non-Newtonian rheology of the fluid is an essential component in the formulation. To be stable during storage, we require the initial suspension to have a yield stress, which arises from the network formed between the nanoparticulate plates of the clay. Under the high shear of the inkjet nozzle, the network breaks down and the fluid shear thins such that its Ohnesorge number is within the compatible range of the inkjet printhead. The finite time taken to rebuild the laponite network is also important: if the network rebuilds too quickly, the droplet will gel before it begins to dry and a domed deposit will result; if it is too slow the droplet will gel too late in the drying process, after the ring stain has begun to form. The recovery time of the network decreases as the laponite concentration increases, and it is the balance of the increasing concentration of laponite during drying and the corresponding decrease in the recovery time that provides the necessary control over the gelling of the droplet.

The presence of laponite in the formulation had a further benefit of pinning the contact line throughout drying and enabling the formation of a circular deposit of well-defined diameter.

The addition of a new component to a formulation can have undesirable side-effects. In this case, we found that laponite was prone to induce aggregation of the latex spheres.

Colloidal silica was found to be a suitable additive for reducing large scale aggregation and providing a smoother surface texture to deposits. However, the colloidal silica reduced the critical strain of the laponite suspensions, which favoured the formation of ring staining. A careful balance of the silica to laponite ratio was needed to ensure a flat deposit profile with reduced aggregation and a smooth surface texture, while maintaining suitable rheological properties for storage and jetting.

Acknowledgement

The authors thank H.N. Yow and S. Biggs (Leeds University, UK) for providing the polystyrene spheres and Zeta potentials. This work was supported financially by EPSRC under grant number EP/H018913/1.

Supporting Information Available

Additional figures and videos. This material is available free of charge via the Internet at `http://pubs.acs.org/`.

References

(1) Hutchings, I. M.; Martin, G. D. *Inkjet Technology for Digital Fabrication*, 1st ed.; Wiley-Blackwell, 2012.

(2) Sobac, B.; Brutin, D. Triple-Line Behavior and Wettability Controlled by Nanocoated Substrates: Influence on Sessile Drop Evaporation. *Langmuir* **2011**, *27*, 14999–15007.

(3) Jokinen, V.; Sainiemi, L.; Franssila, S. Controlled Lateral Spreading and Pinning of Oil Droplets Based on Topography and Chemical Patterning. *Langmuir* **2011**, *27*, 7314–7320.

(4) Léopoldès, J.; Dupuis, A.; Bucknall, D. G.; Yeomans, J. M. Jetting Micron-Scale Droplets onto Chemically Heterogeneous Surfaces. *Langmuir* **2003**, *19*, 9818–9822.

(5) Larsen, S. T.; Taboryski, R. A Cassie-Like Law Using Triple Phase Boundary Line Fractions for Faceted Droplets on Chemically Heterogeneous Surfaces. *Langmuir* **2009**, *25*, 1282–1284.

(6) Deegan, R. D. Pattern Formation in Drying Drops. *Phys. Rev. E* **2000**, *61*, 475–485.

(7) Maheshwari, S.; Zhang, L.; Zhu, Y.; Chang, H.-C. Coupling Between Precipitation and Contact-Line Dynamics: Multiring Stains and Stick-Slip Motion. *Phys. Rev. Lett.* **2008**, *100*, 044503.

(8) Sangani, A. S.; Lu, C.; Su, K.; Schwarz, J. A. Capillary Force on Particles Near a Drop Edge Resting on a Substrate and a Criterion for Contact Line Pinning. *Phys. Rev. E* **2009**, *80*, 011603.

(9) Deegan, R. D.; Bakajin, O.; Dupont, T. F.; Huber, G.; Nagel, S. R.; Witten, T. A. Contact Line Deposits in an Evaporating Drop. *Phys. Rev. E* **2000**, *62*, 756–765.

(10) Faers, M. A.; Pontzen, R. Factors Influencing the Association between Active Ingredient and Adjuvant in the Leaf Deposit of Adjuvant-Containing Suspoemulsion Formulations. *Pest Manag. Sci.* **2008**, *64*, 820–833.

(11) Shen, X.; Ho, C.-M.; T.-S.Wong, Minimal Size of Coffee Ring Structure. *J. Phys. Chem. B* **2010**, *114*, 5269–5274.

(12) Dou, R.; Wang, T.; Guo, Y.; Derby, B. Ink-Jet Printing of Zirconia: Coffee Staining and Line Stability. *J. Am. Ceram. Soc.* **2011**, *94*, 3787–3792.

(13) Friederich, A.; Binder, J. R.; Bauer, W. Rheological Control of the Coffee Stain Effect for Inkjet Printing of Ceramics. *J. Am. Ceram. Soc.* **2013**, *1*, 1–7.

(14) Deegan, R. D.; Bakajin, O.; Dupont, T. F.; Huber, G.; Nagel, S. R.; Witten, T. A. Capillary Flow as the Cause of Ring Stains from Dried Liquid Drops. *Nature* **1997**, *389*, 827–829.

(15) Talbot, E. L.; Berson, A.; Bain, C. D. Drying and Deposition of Picolitre Droplets of Colloidal Suspensions in Binary Solvent Mixtures. *NIP28: 28th International Conference on Digital Printing Technologies, and Digital Fabrication 2012, September 2012, The Society for Imaging Science and Technology* **2012**, 420–423.

(16) Talbot, E. L.; Berson, A.; Bain, C. D. Internal Flows and Particle Transport Inside Picoliter Droplets of Binary Solvent Mixtures. *NIP29: 29th International Conference on Digital Printing Technologies, and Digital Fabrication 2013, September/October 2013, The Society for Imaging Science and Technology* **2013**, *28*, 307–312.

(17) Vaseem, M.; Lee, K. M.; Hong, A.-R.; Hahn, Y.-B. Inkjet Printed Fractal-Connected Electrodes with Silver Nanoparticle Ink. *Appl. Mater. Interfaces* **2012**, *4*, 3300–3307.

(18) Fribourg-Blanc, E.; Dang, D. M. T.; Dang, C. M. Characterization of Silver Nanoparticle Based Inkjet Printed Lines. *Microsyst. Technol.* **2013**, *19*, 1961–1971.

(19) Wang, B.-Y.; Yoo, T.-H.; Song, Y.-W.; Lim, D.-S.; Oh, Y.-J. Cu Ion Ink for a Flexible Substrate and Highly Conductive Patterning by Intensive Pulsed Light Sintering. *Appl. Mater. Interfaces* **2013**, *5*, 4113–4119.

(20) Roth, E. A.; Xu, T.; Das, M.; Gregory, C.; Hickman, J. J.; Boland, T. Inkjet Printing for High-Throughput Cell Patterning. *Biomater.* **2004**, *25*, 3707–3715.

(21) Ko, S. H.; Pan, H.; Grigoropoulos, C. P.; Luscombe, C. K.; Fréchet, J. M. J.; Poulikakos, D. All-Inkjet-Printed Flexible Electronics Fabrication on a Polymer Substrate by Low-Temperature High-Resolution Selective Laser Sintering of Metal Nanoparticles. *Nanotech.* **2007**, *18*, 1–8.

(22) Schirmer, N. C.; Ströhle, S.; Tiwari, M. K.; Poulikakos, D. On the Principles of Printing Sub-micrometer 3D Structures from Dielectric-Liquid-Based Colloids. *Adv. Func. Mater.* **2011**, *21*, 388–395.

(23) Park, J.; Moon, J. Control of Colloidal Particle Deposit Patterns within Picoliter Droplets Ejected by Ink-Jet Printing. *Langmuir* **2006**, *22*, 3506–3513.

(24) Kajiya, T.; Kobayashi, W.; Okuzono, T.; Doi, M. Controlling the Drying and Film Formation Processes of Polymer Solution Droplets with Addition of Small Amount of Surfactants. *J. Phys. Chem. B* **2009**, *113*, 15460–15466.

(25) Kim, D.; Jeong, Y.; Koo, C. Y.; Song, K.; Moon, J. Thin Film Transistors with Ink-Jet Printed Amorphous Oxide Semiconductors. *Jap. J. App. Phys.* **2010**, *49*, 05EB06.

(26) Cui, L.; Zhang, J.; Zhang, X.; Huang, L.; Wang, Z.; Li, Y.; Gao, H.; Zhu, S.; Wang, T.; Yang, B. Suppression of the Coffee Ring Effect by Hydrosoluble Polymer Additives. *Appl. Mater. Interfaces* **2012**, *47*, 2775–2780.

(27) Soltman, D.; Subramanian, V. Inkjet-Printed Line Morphologies and Temperature Control of the Coffee Ring Effect. *Langmuir* **2008**, *24*, 2224–2231.

(28) Hendarto, E.; Gianchandani, Y. B. Size Sorting of Floating Spheres Based on Marangoni Forces in Evaporating Droplets. *J. Micromech. Microeng.* **2013**, *23*, 1–7.

(29) Kim, S. J.; Kang, K. H.; Lee, J.-G.; Kang, I. S.; Yoon, B. J. Control of Particle-Deposition Pattern in a Sessile Droplet by Using Radial Electroosmotic Flow. *Anal. Chem.* **2006**, *78*, 5192–5197.

(30) Ko, S. H.; Lee, H.; Kang, K. H. Hydrodynamic Flows in Electrowetting. *Langmuir* **2008**, *24*, 1094–1101.

(31) Eral, H. B.; Augustine, D. M.; Duits, M. H. G.; Mugele, F. Suppressing the Coffee

Stain Effect: How to Control Colloidal Self-Assembly in Evaporating Drops using Electrowetting. *Soft Matter* **2011**, *7*, 4954–4958.

(32) Hu, H.; Larson, R. G. Analysis of the Effects of Marangoni Stresses on the Microflow in an Evaporating Sessile Droplet. *Langmuir* **2005**, *21*, 3963–3971.

(33) Hu, H.; Larson, R. G. Marangoni Effect Reverses Coffee-Ring Depositions. *J. Phys. Chem. B* **2006**, *110*, 7090–7094.

(34) Hamamoto, Y.; Christy, J. R. E.; Sefiane, K. The Flow Characteristics of an Evaporating Ethanol Water Mixture Droplet on a Glass Substrate. *J. Therm. Sci. Technol.* **2012**, *7*, 425–436.

(35) Ristenpart, W. D.; Kim, P. G.; Domingues, C.; Wan, J.; Stone, H. A. Influence of Substrate Conductivity on Circulation Reversal in Evaporating Drops. *Phys. Rev. Lett.* **2007**, *99*, 234502.

(36) Lim, J. A.; Lee, W. H.; Lee, H. S.; Lee, J. H.; Park, Y. D.; Cho, K. Self-Organization of Ink-jet-Printed Triisopropylsilylethynyl Pentacene via Evaporation-Induced Flows in a Drying Droplet. *Adv. Funct. Mater.* **2008**, *18*, 229–234.

(37) de Gans, B.-J.; Schubert, U. S. Inkjet Printing of Well-Defined Polymer Dots and Arrays. *Langmuir* **2004**, *20*, 7789–7793.

(38) Truskett, V. N.; Stebe, K. J. Influence of Surfactants on an Evaporating Drop: Fluorescence Images and Particle Deposition Patterns. *Langmuir* **2003**, *19*, 8271–8279.

(39) Still, T.; Yunker, P. J.; Yodh, A. G. Surfactant-Induced Marangoni Eddies Alter the Coffee-Rings of Evaporating Colloidal Drops. *Langmuir* **2012**, *28*, 4984–4988.

(40) Cox, W. R.; Chen, T.; Guan, C.; Hayes, D. J.; Hoenigm, R. E.; Teipen, B. T.; MacFarlane, D. Micro-jet Printing of Refractive Microlenses. *Proceedings OSA Diffractive Optics and Micro-Optics Topical Meeting, Kailua-Kona, Hawaii, June* **1998**,

(41) van den Berg, A. M. J.; de Laat, A. W. M.; Smith, P. J.; Perelaera, J.; Schubert, U. S. Geometric Control of Inkjet Printed Features using a Gelating Polymer. *J. Mater. Chem.* **2007**, *17*, 677–683.

(42) Sun, K.; Raghavan, S. R. Thermogelling Aqueous Fluids Containing Low Concentrations of Pluronic F127 and Laponite Nanoparticles. *Langmuir* **2010**, *26*, 8015–8020.

(43) Alfred, D. R. (Dataproducts Corporation). Formulation for Depositing a Material on a Substrate using Ink Jet Printing. European Patent 0329026B1, 1993.

(44) Mourchid, A.; Delville, A.; Levitz, P. Sol-Gel Transition of Colloidal Suspensions of Anisotropic Particles of Laponite. *Faraday Discuss.* **1995**, *101*, 275–285.

(45) Hoath, S. D.; Jung, S.; Hsiao, W.-K.; Hutchings, I. M. How PEDOT:PSS Solutions Produce Satellite-Free Inkjets. *Organic Electronics* **2012**, *13*, 3259–3262.

(46) Hu, H.; Larson, R. G. Evaporation of a Sessile Droplet on a Substrate. *J. Phys. Chem. B* **2002**, *106*, 1334–1344.

(47) `www.http://physics.georgetown.edu/matlab/tutorial.html.Viewed15/07/2013.`

(48) Joshi, Y. M.; Ranjith, G.; Reddy, K.; Kulkarni, A. L.; Kumar, N.; Chhabra, R. P. Rheological Behaviour of Aqueous Suspensions of Laponite: New Insights into the Ageing Phenomena. *Proc. R. Soc. A* **2008**, *464*, 469–489.